Influence of an electric field on the optical properties of few-layer graphene with *AB* stacking

C. L. Lu,[1] C. P. Chang,[2,5,*] Y. C. Huang,[1,3] R. B. Chen,[4] and M. L. Lin[1,5,†]
[1]*Department of Physics, National Cheng Kung University, 701 Tainan, Taiwan*
[2]*Center for General Education, Tainan Woman's College of Arts and Technology, 710 Tainan, Taiwan*
[3]*Center for General Education, Kao Yuan University of Technology, 821 Kaohsiung, Taiwan*
[4]*Center for General Education, National Kaohsiung Marine University, 830 Kaohsiung, Taiwan*
[5]*National Center for Theoretical Sciences, Taiwan*
(Received 3 November 2005; revised manuscript received 26 January 2006; published 24 April 2006)

The effect of perpendicular electric field (**F**) on optical properties of the *AB*-stacked few-layer graphene, made up of two, three, or four graphite sheets, is explored through the gradient approximation. In contrast to the featureless optical spectra of graphene, the low-energy absorption spectra of few-layer graphene with *AB* stacking exhibit many jumping structures, which result from the band-edge states caused by the stacking effect, in the absence of an electric field. Remarkably, **F** causes the subband (anti)crossing, changes the subband spacing, produces the oscillating bands, and increases the band-edge states. It, therefore, follows that the field-modulating spectra with sharp peaks are generated. Moreover, the frequency of peak, which is strongly dependent on the layer number and the field strength, is predicted. Above all, the predicted absorption spectra and the associated electronic properties could be verified by the optical measurements.

DOI: 10.1103/PhysRevB.73.144427 PACS number(s): 73.20.At, 73.61.−r, 78.20.−e

I. INTRODUCTION

The layered graphites have attracted a lot of studies, mainly owing to the special geometric structures.[1] They exhibit very rich physical properties, e.g., electronic properties and optical excitations. The main features of electronic structures are directly reflected in optical properties. Graphite crystals are the arrangement of hexagonal graphite sheets, held by the van der Walls forces, in the *AA*, *AB*, or *ABC* sequence along the z axis. In general, natural graphite adopts an *AB*-stacking sequence.[2–4] Graphite sheet (graphene) is an atomic monolayer composed of the hexagonal rings of carbon atoms with strong σ bonds. The p_z orbitals, perpendicular to graphite plane, cause the special electronic properties—two linear energy dispersions touching each other at the Fermi energy (E_F). A graphite sheet is a zero-gap semiconductor with the vanishing density of state (DOS) at E_F. Due to the geometric structure and the interlayer interactions, the *AB*-stacked graphite show anisotropic energy dispersions along the stack direction. The interlayer interactions markedly change the energy dispersions at low energy[1–7] and lead to the nonvanishing value of DOS at E_F.

Because of the progress of fabrication technology, various graphite-based materials, such as one-dimensional (1D) nanotubes,[8] 0D carbon toroids,[9] 1D nanographite monoribbon,[10] and 2D nanographite multiribbons,[11,12] are produced. 1D nanotubes can be obtained from the rolling of a graphite sheet to a cylinder shape. By segmenting a long nanotube, a finite nanotube forms. A 0D carbon toroid is the connection of two ends of finite 1D nanotube in the ring form. In contrast to these tubular systems, 2D nanographite multiribbons (1D nanographite monoribbon) can be regarded as the slit of a graphite crystal (graphite sheet). By reducing the dimensionality in the graphite basal planes, such planar systems come about. Through the change in the dimensionality and the size of materials, the peculiar electronic properties of these tubular and planar systems emerge. The findings are, therefore, triggering more ideas. Another option is to reduce the dimensionality of graphite along the c axis. More recently, the stack of finite layers of graphene along the c axis, namely, few-layer graphene (FLG), is produced, for example, through the exfoliation of the small mesa of highly oriented pyrolytic graphite.[13] The experimental measurement shows that FLG is stable under ambient conditions and that FLG is a 2D semimetal with a light overlap between valence bands and conduction bands.[13] The FLG has also been used to fabricate the device such as the field effect transistor.[13–16]

It is well known that the electric field can effectively modify both electronic and transport properties of low-dimensional systems, e.g., 1D quantum wires,[17] and 1D carbon nanotubes.[18–22] The influence of electric field on the physical properties of the quasi-two-dimensional FLG is to be expected. In a previous work of ours,[23] the dependence of electronic properties on the geometric structure (the number of layers and the interlayer interactions) and the electric field is investigated in detail. First, it is found that the interlayer interactions destroy symmetry and isotropy of energy bands and change linear bands into parabolic bands. They also remarkably cause the weak overlap between valence and conduction bands in bilayer (four-layer) graphene. Then, the perpendicular electric field can give rise to the subbands (anti)crossing, change the subband spacing, induce the oscillating bands, and increase the band-edge states. Remarkably, bilayer graphene makes a transition from semimetal to semiconductor with a band gap significantly modulated by the electric field. More importantly, the effects caused by geometric structure and electric field—the induction of two kinds of special structures, the shift of peak position, the change of peak height, and the alternation of band gap—are revealed in DOS.

Above all, the calculation of optical properties makes it possible for us to investigate the aforementioned electronic properties. The spectroscopy[24] could be used to examine the

 ©2006 The American Physical Society

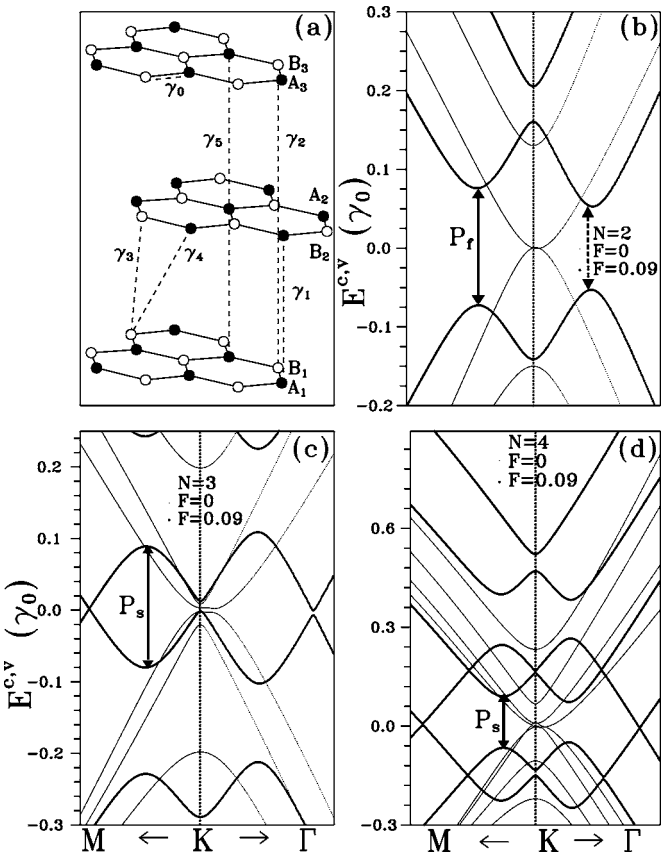

FIG. 1. (a) The geometric structure of the trilayer graphene. γ_0 is the intralayer interaction and γ_i's indicate the interlayer interactions. The light (heavy) curves in (b), (c), and (d), respectively, exhibit the energy dispersions of the bilayer, trilayer, and four-layer graphene in the absence (presence) of electric field with the unit of $\gamma_0/(e\text{Å})$. The ranges of wave number along the KM and $K\Gamma$ directions are, respectively, 0.1 $K_{\max}$ in (b), 0.09 $K_{\max}$ in (c), and 0.15 $K_{\max}$ in (d), where $K_{\max}$ is the magnitude of wave vector pointing from the point K to the point Γ of the first Brillouin zone.

calculated absorption spectra, which respond directly to the main features of electronic structures. By employing the gradient approximation, the optical properties of FLG with layer number $N=2$, 3, and 4 are explored in this work. This paper is organized as follows. In Sec. II, the analytic Hamiltonian matrix elements of the tight-binding method for electronic properties of FLG are first derived. The effects of geometric structure and electric field on the low-energy absorption spectra are then investigated in Sec. III. Finally, conclusions are drawn in Sec. IV.

II. THEORY AND METHOD

Figure 1(a) exhibits the geometrical structure and all tight-binding parameters of *AB*-stacked graphite, where two atoms, denoted as A_i and B_i, exist in the primitive cell of each graphene. In the *AB* order, half of atoms (A_i) lie directly above each other in the adjacent sheets and the other half (B_i) lie above the center of the hexagons in the adjacent layers. The C-C bond length in the graphite plane is $b=1.42$ Å. The distance between the two nearest neighboring sheets is $c=3.35$ Å.[2] The tight-binding parameters shown in Fig. 1 are as follows. That between A and B atoms on the same graphite layer is γ_0. The interaction between two A atoms from two neighboring layers is γ_1. That between two B atoms from two neighboring layers is γ_3. γ_4 represents the interaction between atom A and B from two neighboring layers. The hopping integral γ_5 is the interaction between two A atoms from the two next-neighboring planes. γ_2 is the interaction between two B atoms from the two next-neighboring planes. The atoms A form the linear atom chains along the stacking direction, while the atoms B form the zigzag textures along that direction. Therefore, the second neighboring interaction γ_5 is different from γ_2. Moreover, the local chemical environment of atom A is dissimilar to that of atom B. The different chemical environment between atom A and atom B is reflected in the site energy γ_6. The values of γ_0 and γ_i's are[2] $\gamma_0=2.598$ eV, $\gamma_1=0.364$ eV, $\gamma_2=-0.014$ eV, $\gamma_3=0.319$ eV, $\gamma_4=0.177$ eV, $\gamma_5=0.036$ eV, and $\gamma_6=-0.026$ eV. The *AB* stacked N-layer graphene can be looked upon as the extraction of the *AB*-stacked graphite. From this point of view, Fig. 1(a) also represents the geometrical structure of trilayer graphene. $2N$ atoms $(A_1,B_1,A_2,B_2,\ldots,A_N,B_N)$ are found in the unit cell of the N-layer graphene with *AB* stacking. For simplicity, all the tight-binding parameters of the *AB*-stacked graphite are directly used to simulate these FLG systems.

An electric field $(\mathbf{F})$ perpendicular to graphite planes is used to modulate the electronic states of an FLG. For the sake of calculation convenience, $\mathbf{F}$ is assumed not to affect the rigid structure and, thus, not the tight-binding parameters of the FLG. The $2p_z$ orbitals are fully to describe the π-electronic states that exactly dominate the low-energy electronic properties. The σ bands are omitted because they are far apart from the Fermi energy. Because of the screening effect,[25,26] $\mathbf{F}$ is an effective field, which is only to add an electric potential $U=-e\mathbf{F}z$ on the site energy of a carbon atom. The Hamiltonian equation is

$$H|\Psi\rangle = E|\Psi\rangle, \tag{1}$$

where $|\Psi\rangle$ is the wave function, which is presented as the linear combination of the Bloch function $|A\rangle$ and $|B\rangle$. In bracket notation, the wave function is

$$|\Psi\rangle = a_1|A_1\rangle + b_1|B_1\rangle + a_2|A_2\rangle + \cdots + a_N|A_N\rangle + b_N|B_N\rangle. \tag{2}$$

Within the frame of tight-binding method $|A_i\rangle$ and $|B_i\rangle$, the Bloch functions for the π bands at the ith graphite sheet are expressed by a linear combination of the atomic $2P_z$ orbitals $\phi(\mathbf{R}_I-\mathbf{r}-\tau_\alpha)$:

$$|\alpha_i\rangle = \sum_{\mathbf{R}_I} e^{i\mathbf{k}\cdot\mathbf{R}_I}\phi(\mathbf{R}_I - r - \tau_\alpha), \tag{3}$$

where α denotes A or B. $\mathbf{R}_I$ is the 3D periodical position vector and $\tau_\mathbf{A}$ and $\tau_\mathbf{B}$ are position vectors in a basis. The representation of Hamiltonian operator is a $2N\times 2N$ Hermitian matrix. Its elements are in the form of $\langle\alpha_i|H|\beta_j\rangle$, where α (β) denotes $|A\rangle$ or $|B\rangle$ and i (j) indicates the graphene

order $1,2,3,\ldots,N$ along the z axis (the stacking direction). The nonzero elements are listed as follows:

$$\langle A_i|H|A_i\rangle = -e\mathbf{F}z_i + \gamma_6,$$

$$\langle A_i|H|B_i\rangle = \gamma_0 f(k_x,k_y),$$

$$\langle B_i|H|A_i\rangle = \gamma_0 f^*(k_x,k_y),$$

$$\langle B_i|H|B_i\rangle = -e\mathbf{F}z_i, \quad \text{if } i \text{ is odd}. \tag{4}$$

They are also the elements of Hamiltonian matrix of the ith graphite sheet along the z axis when i is odd. Here $f(k_x,k_y) = \Sigma_{l=1}^{3}\exp(i\mathbf{k}\cdot\mathbf{b}_l)$, where $\mathbf{b}_l$ represents the nearest neighbor in the same graphite plane and $\mathbf{k}=(k_x,k_y)$ is the wave vector. The effective electric field chiefly adds an electric potential $-e\mathbf{F}z_i$ to the site energy of carbon atoms, where z_i is the z coordinate of the ith graphite plane and is equal to $z_i=(i-1)c$. It should be noted that due to the stacking effect the elements of Hamiltonian matrix of the other half graphite sheets are

$$\langle A_i|H|A_i\rangle = -e\mathbf{F}z_i + \gamma_6,$$

$$\langle A_i|H|B_i\rangle = \gamma_0 f^*(k_x,k_y),$$

$$\langle B_i|H|A_i\rangle = \gamma_0 f(k_x,k_y),$$

$$\langle B_i|H|B_i\rangle = -e\mathbf{F}z_i, \quad \text{if } i \text{ is even}.$$

The interlayer interactions between the two nearest-neighbor graphite sheets brings about the nonzero matrix elements

$$\langle A_i|H|A_{i+1}\rangle = \langle A_{i+1}|H|A_i\rangle = \gamma_1,$$

$$\langle A_i|H|B_{i+1}\rangle = \langle B_{i+1}|H|A_i\rangle^* = \gamma_4 f^*(k_x,k_y),$$

$$\langle B_i|H|A_{i+1}\rangle = \langle A_{i+1}|H|B_i\rangle^* = \gamma_4 f^*(k_x,k_y),$$

$$\langle B_i|H|B_{i+1}\rangle = \langle B_{i+1}|H|B_i\rangle^* = \gamma_3 f(k_x,k_y). \tag{5}$$

The matrix elements resulting from the second-neighbor interactions γ_5 and γ_2 are

$$\langle A_i|H|A_{i+2}\rangle = \langle A_{i+2}|H|A_i\rangle = \gamma_5,$$

$$\langle B_i|H|B_{i+2}\rangle = \langle B_{i+2}|H|B_i\rangle = \gamma_2. \tag{6}$$

Energy dispersions $E^h(k_x,k_y)$ in units of γ_0 and the related wave functions $|\Psi^h(k_x,k_y)\rangle$ are obtained through the diagonalization of Hamiltonian matrix, where $h=c$ (or $h=v$) and c (v) represents the unoccupied (occupied) states. Furthermore, the optical absorption function of an FLG is directly obtained through

$$A(\omega) \propto \sum_{h,h',J,J'} \int_{1stBZ} \frac{dk_x}{2\pi}\frac{dk_y}{2\pi} \times \left| \langle \Psi^{h'}(k_x,k_y,J')|\frac{\hat{\mathbf{E}}\cdot\vec{P}}{m_e}|\Psi^h(k_x,k_y,J)\rangle \right|^2 \times \mathrm{Im}\left[\frac{f[E^{h'}(k_x,k_y,J')] - f[E^h(k_x,k_y,J)]}{E^{h'}(k_x,k_y,J') - E^h(k_x,k_y,J) - \omega - i\Gamma} \right], \tag{7}$$

where $f[E^h(k_x,k_y,J)]$ is the Fermi-Dirac distribution function. Γ ($=0.001\gamma_0$) is the broadening parameter due to various deexcitation mechanism. For the sake of convenience, the subbands away from E_F are assigned to be the index $J = \pm 1, \pm 2, \ldots, \pm N$, respectively. Here + (−) corresponds to the unoccupied π^* states (the occupied π states). Electrons in the presence of electromagnetic field with $\hat{\mathbf{E}}_x \| \hat{x}$ ($\hat{\mathbf{E}}_y \| \hat{y}$) are excited from the occupied π bands to the unoccupied π^* bands. At $T=0$, only inter-π-band excitations occur. The excitation energy is $\omega_{ex}=E^c(k_x,k_y)-E^v(k_x,k_y)$. The optical selection rules are $\Delta k_x=0$ and $\Delta k_y=0$ because the momentum of photons is almost equal to zero.

$$\langle \Psi(k_x,k_y,J')|\frac{\hat{\mathbf{E}}\cdot\vec{P}}{m_e}|\Psi(k_x,k_y,J)\rangle,$$

the velocity matrix element, is evaluated within the gradient approximation[27–30] (Appendix A). The joint density of states is obtained by setting the velocity matrix element in Eq. (7) to 1. Apparently, the optical properties are sensitive to the electronic properties of FLG, which are greatly affected by the layer number, the interlayer interactions and the electric field.

III. OPTICAL PROPERTIES

First, the electronic properties of FLGs with layer number $N=2$, 3, and 4 are briefly reviewed.[23] As shown by the light curves in Figs. 1(b)–1(d), the band features in the absence of an electric field are quite dissimilar to those of graphene, which exhibits two linear bands crossing each other at E_F. The occupied bands are asymmetric to the unoccupied bands about E_F. The band features are very sensitive to the layer number. The bilayer graphene presents four parabolic bands with band-edge states close to the K point (the corner of the first BZ). Moreover, the valence bands slightly touch the conduction bands [Fig. 1(b)]. The low-energy dispersions of trilayer graphene exhibit the parabolic bands and the weak oscillating bands near E_F [Fig. 1(c)]. At the K point, the state energies near E_F are $E=0$, $\pm\gamma_2$, and $\gamma_6-\gamma_5$. It is clearly seen that the second-neighbor interactions between the first and the third graphite planes γ_2 and γ_5 dominate the state energies at K. The oscillating energy dispersions appear near the K point. Notably, a band gap E_g, the energy space between the band edge of $J=-1$ subband and that of $J=1$ subband, is opened. Thus, the trilayer graphene is a semiconductor. Four-layer graphene presents the parabolic bands [Fig. 1(d)]. The state energies closest to $E=0$ are doubly degenerate at the K

point. The energy spacing between the two degenerate energy levels is equal to $2\gamma_2$. Around the K point, the state degeneracy is just destroyed. The valence bands lightly contact the conduction bands. Thus, the four-layer graphene is a 2D semimetal. In short, the interlayer interactions cause asymmetry between the occupied states E^v and the unoccupied states E^c, destroy isotropy of energy bands, change linear bands into parabolic bands, and also remarkably cause weak overlap between the valence and the conduction bands.

The effective electric field leads to the significant changes in energy dispersions, as shown by the heavy curves in Figs. 1(b)–1(d). It is noted that the Fermi level (E_F) of the systems in the presence of electric field is set at the zero energy. The perpendicular electric field $\mathbf{F}$, in units of $\gamma_0/(e\text{Å})$, can open a band gap, cause the subband (anti)crossing, alter the band feature, change the band spacing, and produce new band-edge states as well. First, the electric field not only changes the parabolic bands into the oscillating bands but also induces a band gap in the bilayer graphene [the heavy curves in Fig. 1(b)]. That is to say, the semimetal-semiconductor transition occurs. In contrast to the bilayer graphene, the oscillating bands of trilayer graphene, caused by $\mathbf{F}$, cross (anticross) each other at the certain wave vector along the KM ($K\Gamma$) [the heavy curves in Fig. 1(c)]. The electric field induces the semiconductor-metal transition in the trilayer graphene. The features of oscillating bands—the period and the amplitude—are very sensitive to the layer number [Figs. 1(c) and 1(d)]. Above all, the cooperation between electric field and geometric structures causes the oscillating bands and, thus, produces the new band-edge states near E_F. It is expected that the characteristics of energy dispersions (the oscillating band dispersions and the band-edge states) will reflect on absorption spectra of FLG.

The possible transition channels are all revealed in the features of joint density of states (JDOS). In the absence of electric field, JDOS of FLG with $N=2$, 3, and 4 increases from $\omega=0$ to $\omega=0.5\gamma_0$ [Fig. 2(a)] due to the logarithmic peak at $\omega\approx 2\gamma_0$, which originates in the transition from π band near $-\gamma_0$ to π^* band near γ_0.[23,31,32] The magnitude of JDOS is in proportion to $N\times N$, the possibility of transition channels. JDOS follows a similar trend as seen in the graphite sheet and the AB-stacked graphite. However, JDOS of FLG exhibits many special jumping structures, which are related to the local minima (or maxima) in energy dispersions [the light curves in Figs. 1(b)–1(d)]. Such jumping structures do not appear in JDOS of a graphite sheet. The chief cause is that the graphene presents two linear bands resulting in featureless JDOS near E_F.

JDOS near E_F [the inset in Fig. 2(a)] merits a closer study. They are related to the electronic properties, which are strongly dependent on the geometrical structure. The logarithmic peak of bilayer graphene originates in the saddle point in the energy dispersions. The sharp peak of trilayer graphene results from the nearly flat bands near E_F. The peak position is equal to the band gap E_g of the system [the light curves in Fig. 1(c)]. However, the four-layer graphene exhibits quite dissimilar low-energy JDOS, which only show the oscillating feature. There is no sharp peak or band gap.

The absorption spectra $A(\omega)$ [Fig. 2(b)] are calculated through $A(\omega)=(A_x+A_y)/2$, i.e., the average of A_x and A_y,

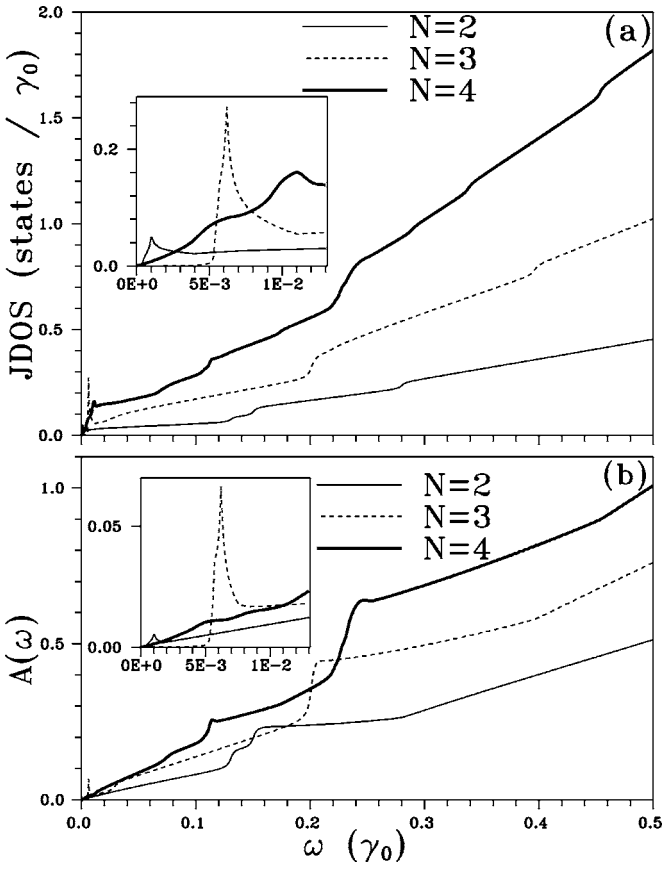

FIG. 2. (a) Joint density of states of the N-layer graphene in the absence of an effective electric field are exhibited for $N=2$, 3, and 4, respectively. The corresponding absorption spectra are shown in (b).

which are absorption spectra in the application of polarized field $\hat{\mathbf{E}}_x \| \hat{x}$ and $\hat{\mathbf{E}}_y \| \hat{y}$, respectively. In the absence of perpendicular electric field, $A(\omega)$ grow from $\omega=0$ to $\omega=0.5\gamma_0$. The feature of spectra is very similar to that of corresponding JDOS, and is proportional to JDOS as well. Spectra chiefly exhibit several discontinuities (or jumping structures). However, the number of discontinuities is less than that of JDOS because the inclusion of velocity matrix closes some transition channels. The inset in Fig. 2(b) shows that the spectra near E_F are similar in structure to JDOS.

The effective electric field alters the aspects of JDOS and induces the striking peaks in JDOS (Fig. 3). The chief cause is that $\mathbf{F}$ significantly modifies the low-energy dispersions, e.g., the change of the band spacing, the alternation of the band feature, the production of oscillating band, and the generation of new band-edge states. In other words, the application of $\mathbf{F}$ leads to the new excitation channels and, therefore, gives rise to these peaks. JDOS of bilayer graphene [Fig. 3(a)] shows that a band gap, whose size varies with field strength, is opened. The first (second) peak [P_f (P_s)] in the form of logarithmic (asymmetric) divergence is related to the saddle point (the band-edge states at the K point) in the energy dispersions [the solid curves in Fig. 2(b)]. However, no band gap is found in the tri- (four-)layer graphene. Additionally, these two systems exhibit JDOS with similar features

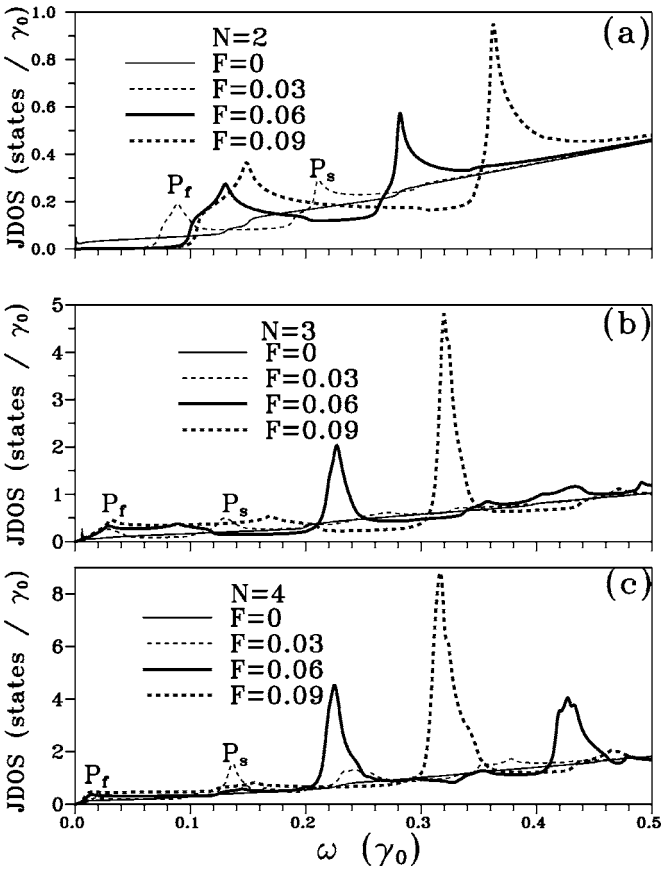

FIG. 3. The light, dashed, heavy, and heavy dashed curves in (a), (b), and (c) show joint density of states of the N-layer graphene (N=2, 3, and 4) under the electric field with the different strength, respectively. **F** is in units of $\gamma_0/(e\text{Å})$.

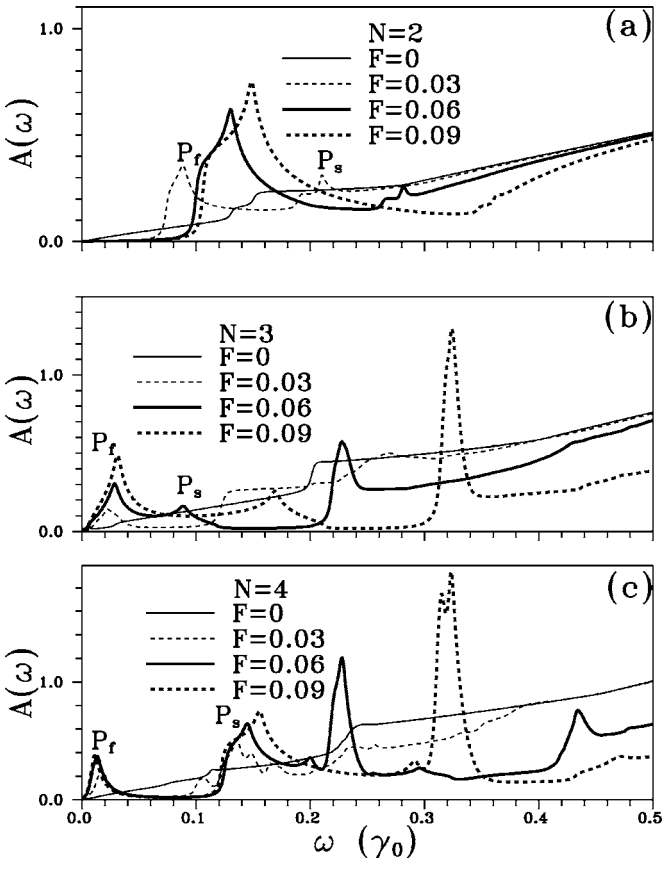

FIG. 4. The absorption spectra of the N-layer graphene in the presence of effective electric field with various strength are shown for N=2, 3, and 4 in (a), (b), and (c), respectively. **F** is in units of $\gamma_0/(e\text{Å})$.

displayed in the presence of strong field, e.g., **F**=0.06 and 0.09.

The electric field **F** has a great effect on the absorption spectra. First, **F** not only opens a band gap but also induces a sharp peak in the low-energy spectra of bilayer graphene [Fig. 4(a)]. The feature of absorption spectra in the energy region from ω=0 to $0.2\gamma_0$ is in proportion to JDOS [Figs. 2(a) and 3(a)]. In the application of strong field, however, spectra are featureless in the energy region $\omega \geqslant 0.3\gamma_0$ because some transition channels in JDOS [Fig. 2(a)] are closed by the vanishing of velocity matrix. In the presence of **F**, the steep rise of the spectra, due to the transition between the band-edge states of $J=-1$ and that of $J=1$ subband [the dashed arrow in Fig. 1(b)], can be used to determine the size of energy gap E_g. The first peak (P_f), made up of two subpeaks, is a compound one. The transition channels of these two subpeaks are indicated, respectively, by the dashed and the solid arrows in Fig. 1(b). The former transition produces a shoulder on the low energy side of the first peak. Hence, the main peak resulting from the saddle point in energy dispersions is in the logarithmic form. The frequency of the first peak P_f depends on the field strength. The second peak (P_s) comes from the transition from local minimum of $J=-1$ subband to band-edge state of $J=2$ subband on the K point [Fig. 1(b)]. This peak makes a blueshift in the increasing of field strength.

The absorption spectra also depend on the layer number. The comparison between Figs. 4(b) and 3(b) shows that spectra of the trilayer graphene at $\omega \geqslant 0.2\gamma_0$ are proportional to the related JDOS, i.e., these transition channels survive in the presence of **F**. However, the spectra at $\omega \leqslant 0.2\gamma_0$, considerably modified by dipole matrix element, are dissimilar to the corresponding JDOS. Owing to the effect caused by the geometric structure, spectra of trilayer graphene [Fig. 4(b)] are quite different from those of bilayer graphene [Fig. 4(a)]. No energy gap is found in the former spectra, in which P_f, close to zero, is in the form of logarithmic divergence. The peak position is affected by the field strength and γ_2, the interaction from the two next-neighboring planes. Moreover, in the presence of the strong field, a sharp peak exists at $\omega \geqslant 0.2\gamma_0$ in the spectra of trilayer graphene.

Remarkably, the characteristics of spectra of bilayer or trilayer graphene are also found in those of the four-layer graphene. For example, the sharp peak at $\omega \geqslant 0.2\gamma_0$ exists in both four-layer and trilayer graphene [the heavy solid (dashed) curves in Figs. 4(c) and 4(b)] in the application of strong field, e.g., **F**=0.09. It should be noticed that P_s of the four-layer graphene [Fig. 4(c)] is similar to P_f of the bilayer graphene [Fig. 4(a)]. Seemingly, the second peak P_s is also in the logarithmic form. In addition, the frequency of P_f in the spectra of four-layer graphene is almost not affected by the strong field [Fig. 4(c)]. The chief cause for such a result

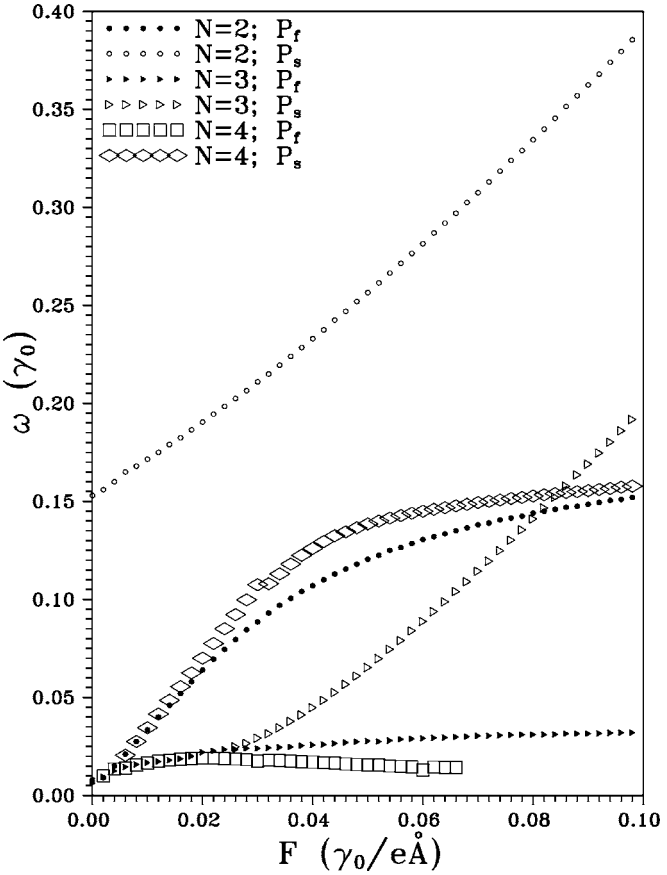

FIG. 5. The frequency of the first and the second absorption peak (ω_f and ω_s) of $N=2$, 3, and 4 FLG vs field strength. The full and empty circles represent ω_f and ω_s bilayer graphene. ω_f (ω_s) of trilayer graphene is shown in the full (empty) triangles. The squares (diamonds) present ω_f (ω_s) of four-layer graphene, respectively.

is that the low-energy electronic properties of FLG with layer number $N=4$ are mainly determined by the interaction γ_2 (γ_5).

The variation of frequency of P_f (P_s) with field strength deserves a thorough examination (Fig. 5). ω_f, the frequency of P_f, of bilayer graphene first grows linearly with the increasing field strength, and it is still increasing at the maximum field (the full circles in Fig. 5). ω_s, the frequency of P_s, of bilayer graphene shows a quite different trend. At a low field strength, ω_s is the parabolic function of field strength **F** (the empty circles in Fig. 5) owing to the competition between lattice potential γ_1 and **F**. However, it is a linear function of **F** at the maximum field. The chief cause is that the excitation energy ω_{ex} of the second peak is dominated by the high field (Appendix B). ω_f and ω_s rely on the geometric structure. As shown by the full triangles in Fig. 5, ω_f of trilayer graphene depends linearly on field strength in the increasing of field strength. It is little affected by a sufficient large field. The second peak (P_s) is generated as the field strength is larger than a threshold (the empty triangles in Fig. 5). The behavior of ω_s of trilayer graphene is similar to that of the bilayer graphene. The empty squares in Fig. 5 show that the electric field influences ω_f of the four-layer graphene in a small degree. However, the intensity of P_f is smeared and cannot be read at a sufficient large field. Notably, the variation of $\omega_s(N=4)$ of the four-layer graphene with field strength (the diamonds in Fig. 5) is very much similar to $\omega_f(N=2)$ of the bilayer graphene (the full circles in Fig. 5).

IV. CONCLUSIONS

In this work, the effect caused by the perpendicular electric field **F** on optical properties of the *AB*-stacked few-layer graphene with layer number $N=2$, 3, and 4 are studied in detail by employing the gradient approximation. In the absence of an electric field, the interlayer interactions, depending on geometric structure, play an important role in energy dispersions. They change the linear bands to parabolic bands and produce new band-edge states. The latter make a good contribution to the absorption spectra. It is found that the low-energy absorption spectra of the few-layer graphene with *AB* stacking exhibit many jumping structures in the absence of an electric field. This behavior is in contrast with the featureless optical spectra of graphene. Then, the electric field **F** strongly modifies the energy dispersions. It can cause the subband (anti)crossing, change the subband spacing, produce the oscillating bands, and increase the band-edge states. Finally, it follows that the sharp peaks are generated in the field-modulating spectra. Moreover, the frequency of peak, which is strongly dependent on the layer number and the field strength **F**, is predicted and explored. And above all, the optical measurements provide a way to verify the predicted absorption spectra and the associated electronic properties.

ACKNOWLEDGMENTS

The authors gratefully acknowledge the support of the Taiwan National Science Council under Contract Nos. NSC 94-2112-M-165-001 and NSC 94-2112-M-006-0002.

APPENDIX A

Based on the gradient approximation,[27–30] the velocity matrix element is expressed as

$$\langle \Psi^{h'}(k_x,k_y,J')|\frac{\hat{\mathbf{E}}\cdot\vec{P}}{m_e}|\Psi^{h}(k_x,k_y,J)\rangle \approx \langle \Psi^{h'}(k_x,k_y,J')|\frac{\partial H}{\partial k}|\Psi^{h}(k_x,k_y,J)\rangle. \quad \text{(A1)}$$

H is the Hamiltonian representation and k is the projection of the wave vector in the direction of electric polarization $\hat{\mathbf{E}}$. Only when Hamiltonian matrix element H_{lm} contains the term $f(k_x,k_y)$, $\partial H_{lm}/\partial k$ is nonzero and equal to $\gamma_{lm}[\partial f(k_x,k_y)/\partial k]$. Inserting the wave function [Eq. (2)] and $\partial H_{lm}/\partial k$ into Eq. (A1) and after some calculation, the square of velocity matrix element has a simple form

$$\left|\langle \Psi^{h'}(k_x,k_y,J')|\frac{\partial H}{\partial k}|\Psi^{h}(k_x,k_y,J)\rangle\right|^2 = \left|\frac{\partial f(k_x,k_y)}{\partial k}\right|^2 |\{\gamma_0[a^{h'*}_{J',1}b^{h}_{J,1}+b^{h'*}_{J',1}a^{h}_{J,1}+\cdots] + \gamma_4[a^{h'*}_{J',1}b^{h}_{J,2}+\cdots]+\gamma_3[b^{h'*}_{J,1}b^{h}_{J,2}+\cdots]\}|^2.$$

As shown in the braces of the above equation, there are three possible channels with great contributions to the optical transition. The electron jumping from the site to its nearest-neighbor site on the same graphite sheet is the first channel, which makes the major contribution to the optical transition. The electron hopping from the site A (B) on one sheet to the site B (A) located on the nearest-neighbor graphite sheet leads to the second channel. The third one results from the electron jumping from the site B on one sheet to the site B located on the nearest-neighbor graphite sheet.

APPENDIX B

The Hamiltonian matrix of bilayer graphene is a 4×4 Hermitian matrix

$$H=\begin{pmatrix} -e\mathbf{F}c/2+\gamma_6 & \gamma_0 f(k_x,k_y) & \gamma_1 & \gamma_4 f^*(k_x,k_y) \\ \gamma_0 f^*(k_x,k_y) & -e\mathbf{F}c/2 & \gamma_4 f^*(k_x,k_y) & \gamma_3 f(k_x,k_y) \\ \gamma_1 & \gamma_4 f(k_x,k_y) & e\mathbf{F}c/2+\gamma_6 & \gamma_0 f^*(k_x,k_y) \\ \gamma_4 f(k_x,k_y) & \gamma_3 f^*(k_x,k_y) & \gamma_0 f(k_x,k_y) & e\mathbf{F}c/2 \end{pmatrix}. \tag{B1}$$

The second peak (P_s) is due to the transition from band-edge state of $J=-1$ subband to that of $J=2$ subband. The band-edge states are very close to the K point. The Hamiltonian matrix at the point K, where $f(k_x,k_y)$ is equal to zero, can be expressed in a simple form

$$H=\begin{pmatrix} -e\mathbf{F}c/2+\gamma_6 & 0 & \gamma_1 & 0 \\ 0 & -e\mathbf{F}c/2 & 0 & 0 \\ \gamma_1 & 0 & e\mathbf{F}c/2+\gamma_6 & 0 \\ 0 & 0 & 0 & e\mathbf{F}c/2 \end{pmatrix}. \tag{B2}$$

Eigenvalues can be analytically obtained. States energies are $E(k_x,k_y,J=\pm1)=\pm|e\mathbf{F}c/2|$ and $E(k_x,k_y,J=\pm2)=\gamma_6 \pm\sqrt{(e\mathbf{F}c/2)^2+\gamma_1^2}$. The optical excitation energy of the second peak (P_s) is $\omega_{ex}\approx E^c(k_x,k_y,J=2)-E^v(k_x,k_y,J=-1)$ and the frequency of the second peak is $\omega_s\approx\gamma_6+\sqrt{(e\mathbf{F}c/2)^2+\gamma_1^2}+|e\mathbf{F}c/2|$. Apparently, ω_s is dependent on the field strength and γ_1. In the presence of the strong electric field, $e\mathbf{F}c/2 \gg \gamma_1$ and ω_s is approximated to $\gamma_6+|e\mathbf{F}c|$.

*Electronic address: t00252@ms.twcat.edu.tw
†Electronic address: mflin@mail.ncku.edu.tw

[1] B. T. Kelly, *Physics of Graphite* (Applied Science, London, 1981).
[2] J. C. Charlier, X. Gonze, and J. P. Michenaud, Phys. Rev. B **43**, 4579 (1991).
[3] J. C. Charlier, J. P. Michenaud, and X. Gonze, Phys. Rev. B **46**, 4531 (1992).
[4] J. C. Charlier, X. Gonze, and J. P. Michenaud, Carbon **32**, 289 (1994).
[5] R. Ahuja, S. Auluck, J. Trygg, J. M. Wills, O. Eriksson, and B. Johansson, Phys. Rev. B **51**, 4813 (1995).
[6] R. C. Tatar and S. Rabii, Phys. Rev. B **25**, 4126 (1982).
[7] E. Mendez, A. Misu, and M. S. Dresselhaus, Phys. Rev. B **21**, 827 (1980).
[8] R. Satio, G. Dresselhaus, and M. S. Dresselhaus, *Physical Properties of Carbon Nanotubes* (Imperial College Press, London, 1998).
[9] C. C. Tsai, F. L. Shyu, C. W. Chiu, C. P. Chang, R. B. Chen, and M. F. Lin, Phys. Rev. B **70**, 075411 (2004).
[10] F. L. Shyu and M. F. Lin, J. Phys. Soc. Jpn. **69**, 3529 (2000).
[11] F. L. Shyu, M. F. Lin, C. P. Chang, R. B. Chen, J. S. Shyu, Y. C. Wang, and C. H. Liao, J. Phys. Soc. Jpn. **70**, 3348 (2001). (The figures for armchair ribbons in this manuscript will be revised because of the numerical calculation errors.)
[12] C. W. Chiu, F. L. Shyu, C. P. Chang, R. B. Chen, and M. F. Lin, J. Phys. Soc. Jpn. **72**, 170 (2003).
[13] K. S. Novoselov, A. K. Geim, S. V. Morozov, D. Jiang, Y. Zhang, S. V. Dubonos, I. V. Grigorieva, and A. A. Firsov, Science **306**, 666 (2004).
[14] J. S. Bunch, Y. Yaish, M. Brink, K. Bolotin, and P. L. McEuen, Nano Lett. **5**, 287 (2005).
[15] Y. H. Wu, B. J. Yang, B. Y. Zong, H. Sun, Z. X. Shen, and Y. P. Feng, J. Mater. Chem. **14**, 469 (2004).
[16] Y. B. Zhang, J. P. Small, W. V. Pontius, and P. Kim, Appl. Phys. Lett. **86**, 073104 (2005).
[17] J. Singh, *Physics of Semiconductors and Their Heterostructures* (McGraw-Hill, New York, 1993).
[18] X. Zhou, H. Chen, and O. Y. Zhong-can, J. Phys.: Condens. Matter **13**, L635 (2001).
[19] Y. H. Kim and K. J. Chang, Phys. Rev. B **64**, 153404 (2001).
[20] J. O'Keeffe, C. Y. Wei, and K. J. Cho, Appl. Phys. Lett. **80**, 676 (2002).
[21] Y. Li, S. V. Rotkin, and U. Ravaioli, Nano Lett. **3**, 183 (2003).
[22] K. H. Khoo, M. S. C. Mazzoni, and S. G. Louie, Phys. Rev. B **69**, 201401(R) (2004).
[23] C. L. Lu, C. P. Chang, Y. C. Huang, J. H. Ho, and M. F. Lin (unpublished).
[24] T. I. Jeon, K. J. Kim, C. Kang, I. H. Maeng, J. H. Son, K. H. An, and Y. H. Lee, J. Appl. Phys. **95**, 5736 (2004).
[25] M. Araidai, Y. Nakamura, and K. Watanabe, Phys. Rev. B **70**, 245410 (2004).
[26] C. P. Chang, Y. C. Huang, C. L. Lu, J. H. Ho, T. S. Li, and M. F. Lin, Carbon **44**, 508 (2006).
[27] J. G. Johnson and G. Dresselhaus, Phys. Rev. B **7**, 2275 (1973).
[28] F. L. Shyu, C. P. Chang, R. B. Chen, C. W. Chiu, and M. F. Lin, Phys. Rev. B **67**, 045405 (2003).
[29] A. Grüneis, R. Saito, G. G. Samsonidze, T. Kimura, M. A. Pimenta, A. Jorio, A. G. Souza Filho, G. Dresselhaus, and M. S. Dresselhaus, Phys. Rev. B **67**, 165402 (2003).
[30] J. Jiang, R. Saito, A. Grüneis, G. Dresselhaus, and M. S. Dresselhaus, Carbon **42**, 3169 (2004).
[31] C. P. Chang, C. L. Lu, F. L. Shyu, R. B. Chen, Y. K. Fang, and M. F. Lin, Carbon **42**, 2975 (2004).
[32] R. Ahuja, S. Auluck, J. M. Wills, M. Alouani, B. Johansson, and O. Eriksson, Phys. Rev. B **55**, 4999 (1997).